DOI: 10.17725/rensit.2022.14.373

Statistical properties of the earth's magnetic field before an earthquake accompanied by a tsunami

Alexander E. Volvach
Crimean Astrophysical Observatory, https://crao.ru/
Nauchny 298688, Crimea, Russian Federation
E-mail: volvach@bk.ru

Lev P. Kogan
Nizhny Novgorod State University of Architecture and Civil Engineering, https://nngasu.ru/
Nizhny Novgorod 603950, Russian Federation
E-mail: l_kog@list.ru

Tatiana M. Zaboronkova
R.E.Alexeev Nizhny Novgorod State Technical University, https://www.nntu.ru/
Nizhny Novgorod 603950, Russian Federation
Institute of Applied Physics of the Russian Academy of Sciences, https://ipfran.ru/
Nizhny Novgorod 603950, Russian Federation
E-mail: t.zaboronkova@rambler.ru

Received 30 October 2022, peer-reviewed 07 November 2022, accepted 14 November 2022

Abstract: **A method for predicting earthquakes accompanied by tsunamis based on changes in the statistical properties of the Earth's magnetic field is proposed. Geomagnetic field is analyzed using the measurements taken a few days before the earthquake in the Pacific Ocean. With the help of a statistical functional, which allows one to study the variations in the level of chaos in the random process, the arising a set of structures with a high degree of determinism is revealed. The properties of these structuews can be interpreted as precursors of an earthquake accompanied by a tsunami.**

Keywords: **earthquake, tsunamis, statistical functionality, precursor of earthquake**

UDC 550.343

Acknowledgments: Work was supported by the Russian Science Foundation (project no. 21-12-00-385). The authors are grateful to IZMIRAN researcher Kanonidi K.Kh. for the provided data of measurements of the Earth's magnetic field.

For citation: Alexander E. Volvach, Lev P. Kogan, Tatiana M. Zaboronkova. Statistical properties of the earth's magnetic field before an earthquake accompanied by a tsunami. *RENSIT: Radioelectronics. Nanosystems. Information Technologies*, 2022, 14(4):373-380. DOI: 10.17725/rensit.2022.14.373.

Contents

1. INTRODUCTION

In [1–3], based on the study of the properties of small-scale fluctuations in the probability density of the magnetic field, the critical frequency of the ionosphere,

and the noise of complex biological systems in seismically active regions, a method was proposed and tested for detecting precursors of approaching earthquakes. The proposed approach makes it possible, in particular, to determine the precursors of seismic events at much shorter time intervals (several days instead of several months) than prediction based on the Gutenberg-Richter theorem [4–8], as well as other statistical approaches [9–12]. In this article, based on the methodology [1-3], the properties of a statistical functional describing the characteristics of small-scale fluctuations in the probability density of the Earth's magnetic field are analyzed. Geomagnetic field measurements were carried out from March 12 to March 16, 2022 at the KNY magnetic variation station (Kanoya), located in southern Japan. The change in the amplitude of fluctuations in the probability density of the geomagnetic field in seismically active regions a few days before of an earthquake is associated with the appearance of a random component in the measurement process, caused, for example, by a fracture of lithospheric plates in the most weakened parts of the earth's crust. Note that this random process is weakly dependent on the background noise due to a set of phenomena that usually take place in the corresponding region of the world.

2. PROBLEM STATEMENT AND SOLUTION METHOD

The purpose of this study is to determine the statistical properties of the Earth's magnetic field, which are precursors of an approaching earthquake accompanied by a tsunami. To identify such precursors, the statistical functional previously introduced and tested in [1] is used:

$$L(n) = \frac{A}{M} \sum_{n=l-(M-1)}^{n} |\Theta_l|, \qquad \Theta_l = \sum_{m=0}^{N-1} P_{m,l}(-1)^m. \tag{1}$$

In formula (1), we take A = 1000 and M = 100 min. The chosen value of the coefficient A makes it possible to pass to the range of values of the functional $L(n)$ convenient for analysis with the specified width M of the averaging time interval. The coefficients $P_{m,l}$ are the probabilities that the values of the auxiliary function $F[x]$ used in the problem fall within the interval

$$F[x(t)]_{\min} + mh \le F[x(t)] \le \le F[x(t)]_{\min} + (m+1)h, \quad 0 \le m \le N-1. \tag{2}$$

Unlike the distribution function of the measured random variable $x = x(t)$, the function $F[x]$ must have a probability density with integrable singularities. Taking into account this requirement, the function $F[x] = \sin[x(t)]$ was chosen for calculations. For the specified type of function $F[x]$ with the discretization interval width h = 0.1, the value of N in (1) is $N = 2h^{-1} = 20$. Statistics (2) based on the results of measurements of the X-, Y- and Z-components of the geomagnetic field (in nT). The duration of any segment of the implementation is 60 seconds, during which 60 measurements of the corresponding component of the magnetic field are carried out. Thus, the value of n in (1) is equal to the number of minutes from the start of measurements at 00:00 03/12/2022 UTC (Coordinated Universal Time) to the current time.

The article shows that the entropy of the geomagnetic field increases with the

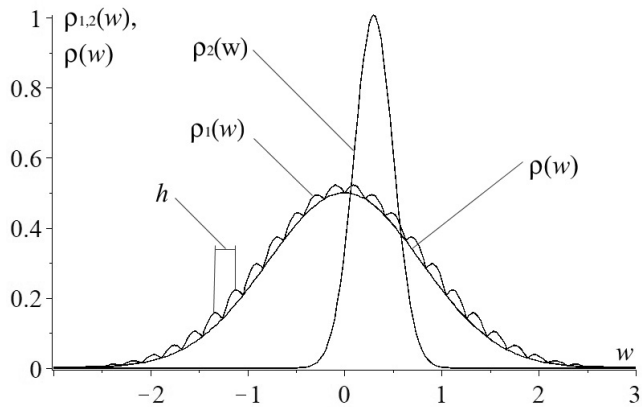

Fig. 1. *Schematic probability distributions* $\rho_1(w)$, $\rho_2(w)$ *and* $\rho(w)$.

approach of an earthquake. Let us explain the above theoretically.

Fig. 1 schematically shows the dependences of the probability density $\rho_1(w)$ and $\rho_2(w)$ for the background noise $x_1(t)$ and, accordingly, the additional (independent of the background noise) random process $x_2(t)$, as well as the probability density $\rho(w)$ of the total random process $x(t) = x_1(t) + x_2(t)$ corresponding to the convolution of the form

$$\rho(w)=\int_{-\infty}^{\infty} \rho_1(w-w')\rho_2(w')dw'.$$

It was theoretically shown in [3] that smoothing of small-scale fluctuations of the curve $\rho_1(w)$ takes place under the condition that the standard of fluctuations of the random variable x_2, which determines the width of the distribution $\rho_2(w)$, is at least several times larger than the sampling interval h, which determines the effective period indicated fluctuations (see Fig. 1).

3. METHOD OF ANALYZING THE RESULTS OF MEASUREMENTS

When analyzing the statistical properties of the magnetic field, the concepts previously introduced in [1] are used: local trends, channels, testing, sliding boundaries. These terms are illustrated by the example in **Fig. 2**, which shows the dependence of the functional $L(n)$ corresponding to measurements of the X-component of the geomagnetic field.

1. Let us call *local trends* the sections of the dependence $L(n)$ located between the points of extrema of this curve and corresponding to variations in δL (the difference between the values of the

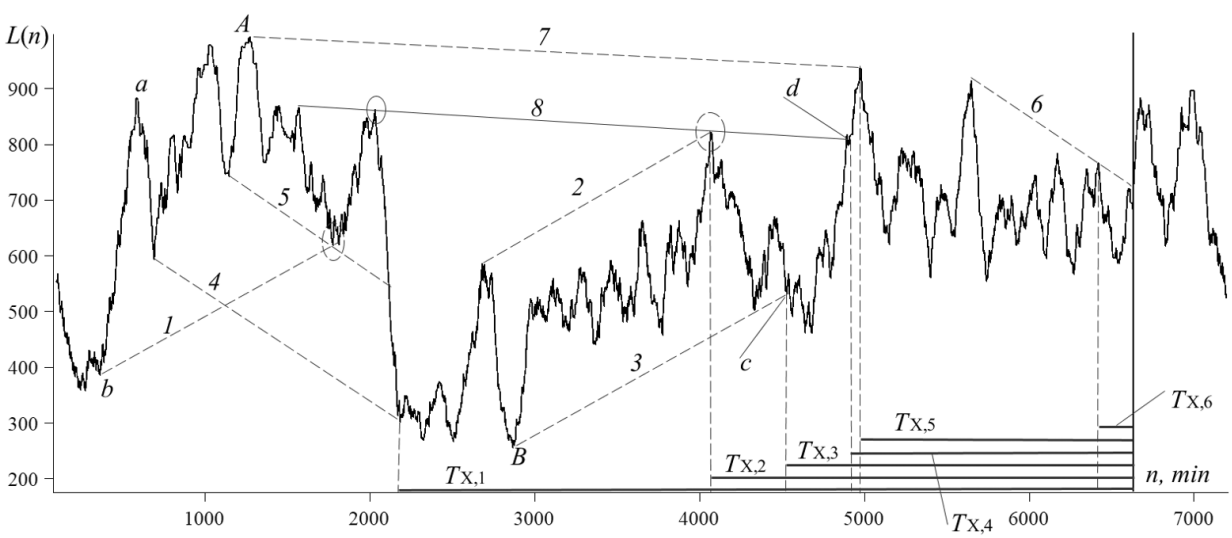

Fig. 2. *Dependence L(n) corresponding to the X-component of the geomagnetic field.*

functional $L(n)$ at the points of maximum and minimum), satisfying the condition $\delta L \geq 0.2\Delta L_{\max}$.

Here $\Delta L_{\max}$ is the maximum variation of the $L(n)$ values throughout a region from the origin to the moment of the earthquake, that is, the difference between the values of the largest minimum and the smallest maximum (respectively, points *A* and *B* in Fig. 2) of the statistical functional $L(n)$ on specified period of time. In this case, the condition is introduced that the geometric deviation ΔS of the curve $L(n)$ from the straight line segment connecting the boundary points of the given local trend satisfies the condition

$$\Delta S \leq 0.2\Delta l, \quad (3)$$

where Δl is the length of this segment. Condition (3) is necessary to ensure the quasi-straightness of the local trend. In Fig. 2 the local trend is, for example, section *ab* of the curve $L(n)$. The points of the boundaries of local trends will be called guiding points. We assume that each such point is horizontally removed from the nearest point of the curve $L(n)$ by no less than the interval $\Delta n = 100$ min.

2. A *channel* is a collection of two lines, each of which passes exactly through two guiding points, and the angle $\Delta\alpha$ between the directions of these lines satisfies the inequality

$$\Delta\alpha \leq 1.4°. \quad (4)$$

In (4), the angle $\Delta\alpha$ is determined using the scalar product of two vectors parallel to the channel boundaries (assuming that the geometric dimensions of the units of the Cartesian axes are equal). The time interval between the guide points through which the channel boundary is drawn must be at least 150 minutes. On Fig. 2 channels are marked: *1–2, 2–3, 4–5, 4–6*, which are formed by two inclined straight segments indicated in the figure by a dotted line. Note that segments *7–8* also form a channel (the properties of its lower boundary *8* will be discussed below).

3. The term *testing* means either the intersection at some point of the curve $L(n)$ and the corresponding channel boundary, or the passing the boundary at a distance ΔL_t vertically from the control point with coordinates $\{n_t, L(n_t)\}$ that satisfies the condition $\Delta L_t \leq 0.012\, L(n_t)$.

As the moment of registration of a precursor of an approaching earthquake, we will consider the time of the last (before the earthquake) testing of the channel boundaries by the dependence $L(n)$ (for example, point *c* for channel *2–3* in Fig. 2).

4. *Sliding boundary* is a straight line drawn through two control points and tested by the $L(n)$ curve at least one more guiding point that satisfies condition (5) (we will call such points additional and highlight them in the figures as a solid ellipse). As in section 3, we assume that the time of registration of the precursor of an approaching earthquake corresponds to the moment of the last testing of this curved line of the sliding boundary (see, for example, point *d* for the sliding boundary *8* in Fig. 2). Sliding boundaries are marked in the figures by solid oblique straight lines.

4. RESULTS OF PROCESSING THE MEASUREMENTS OF THE GEOMAGNETIC FIELD

Figs. 2-4 show the dependences of the functional $L(n)$, which correspond to the measurements of the geomagnetic field

components on the KNY magnetometer located in southern Japan during the period from 00:00 on March 12, 2022 to 23:59 on March 16, 2022. The horizontal axis shows discrete values of time n in minutes $n \geq M = 100$ min counted from the start of measurements. The solid vertical line marks the start of the earthquake with a magnitude of 7.3, which occurred on March 16, 2022 at 14:37 UTC (the epicenter coordinates are 37.702°*N*, 141.587°*E*) and was accompanied by a tsunami.

Fig. 2 corresponds to the dependence $L(n)$ for measurements of the *X*-component of the geomagnetic field. The intervals $T_{X,1} = 4451$ min, $T_{X,2} = 2565$ min, $T_{X,3} = 2104$ min, $T_{X,5} = 1659$ min, and $T_{X,6} = 213$ min correspond to the time intervals between the beginning of the earthquake and the moment of the fifth test for the boundaries of channels *4–5, 1–2, 2–3, 7–8, 4–6*, and the time interval $T_{X,4} = 1743$ min corresponds to the last test point for the sliding boundary *10*. The area near the additional point of the sliding boundary *10* is indicated by a solid ellipse.

Fig. 3 illustrates the dependence $L(n)$ for the *Y*-component of the geomagnetic field. In this case, the intervals $T_{Y,1} = 1896$ min, $T_{Y,2} = 682$ min, $T_{Y,3} = 662$ min, $T_{Y,4} = 662$ min, $T_{Y,5} = 548$ min and $T_{Y,6} = 24$ min. Here $T_{Y,1\text{-}5}$ are the time intervals between the beginning of the earthquake and the moment of the last testing for the boundaries of channels *1–2, 4–5, 6–7*, and *2–3*, and the interval $T_{Y,6}$ corresponds to the last testing of the $L(n)$ curve of the sliding boundary *9*.

In **Fig. 4**, the dependence $L(n)$ corresponds to measurements of the *Z*-component of the geomagnetic field. In this case, there are no sliding boundaries, and the intervals $T_{Z,1} = T_{Z,2} = T_{Z,3} = 1820$ min correspond to the time intervals between the beginning of the earthquake and the moment of the last testing for

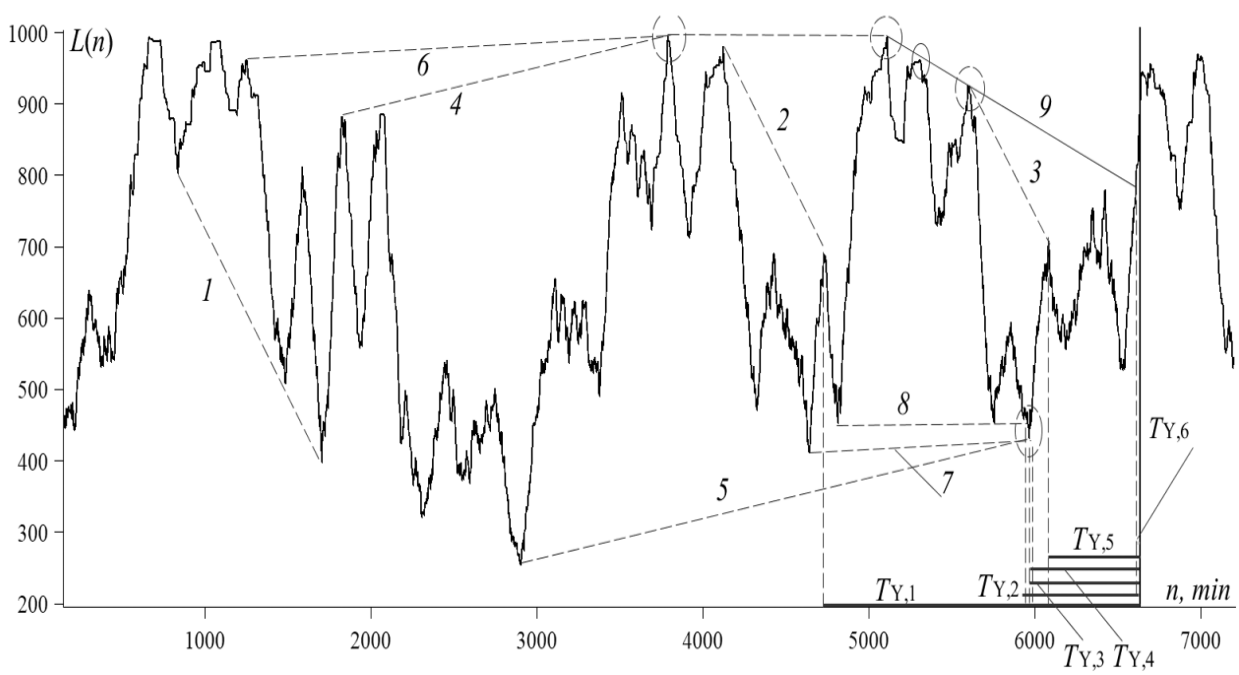

Fig. 3. *Dependence L(n) corresponding to the Y-component of the geomagnetic field.*

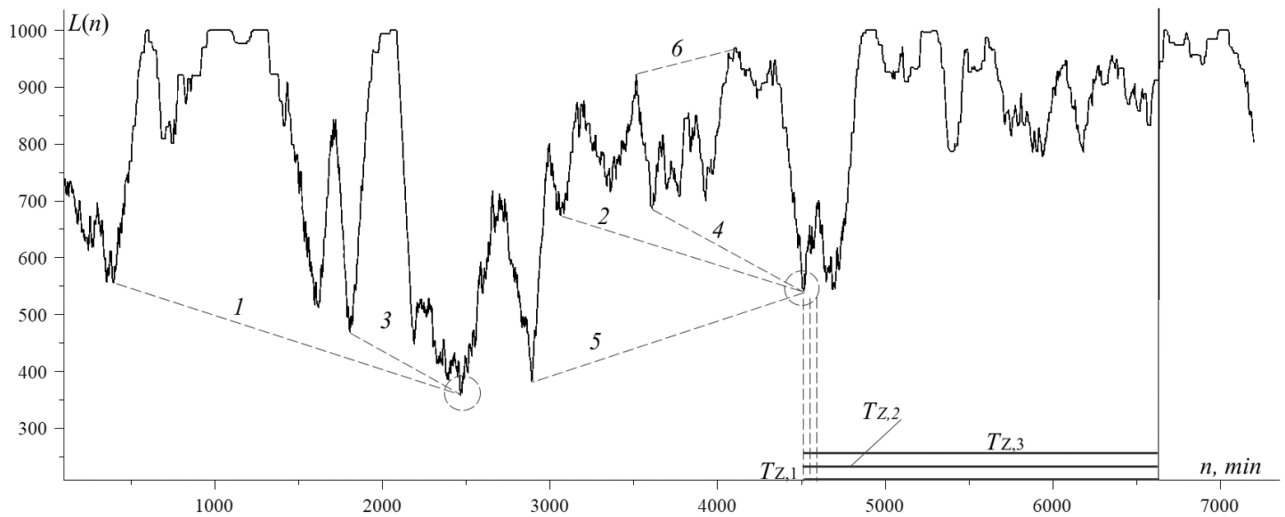

Fig. 4. *Dependence L(n) corresponding to the Z-component of the geomagnetic field.*

the boundaries of channels *1–2, 3–4, 5–6,* respectively.

Note that, as follows from the analysis of Fig. 2–4, before the earthquake, for the *L*(*n*) dependences corresponding to the *X-, Y-,* and *Z*-components of the geomagnetic field, numerous linear structures appeared, similar to those that preceded the seismic events considered in [1-3].

The values indicated in Figures 2-4 of the time intervals from the moment of registration of the precursor to the beginning of the earthquake are given in the **Table**.

As can be seen from the data given in the Table, almost all registered precursors refer to the interval from ten hours to two and a half days before a seismic event. The analysis of behavior of dependences *L*(*n*) showed that the number of precursors in the considered time interval of the order of several days before an earthquake increases in proportion to the duration of the time interval preceding the seismic event.

Table

Time interval values $T_{X,i}$, $T_{Y,i}$ и $T_{Z,i}$.

i	$T_{X,}$, min	$T_{Y,i}$, min	$T_{Z,i}$, min
1	4451	1896	1820
2	2565	682	1820
3	2104	682	1820
4	1743	682	
5	1569	548	
6	213	24	

5. DISCUSSION AND CONCLUSIONS

As a result of the analysis of processing measurements of the geomagnetic field, we come to the following conclusions:

1. For each channel, at least one of its boundaries passes through a critical point belonging to the boundary of another channel. This property indicates the mutual influence of seismic processes at the stage of "final preparation" of an approaching earthquake.
2. A seismic event is preceded by critical points associated with the synchronous or very close in time occurrence of three precursors, defined as the points of the last testing of the corresponding

channels. This can be interpreted as the simultaneous occurrence of three or more processes associated with the "final preparation" of the approaching earthquake.

3. In all presented cases, linear structures of the functional $L(n)$ pass through the point of its deepest minimum. This effect is quite consistent with the theoretical assumption that the specified minimum corresponds to the moment of the greatest compression of the lithospheric plates. Such compression with a high probability can lead to the occurrence of processes of destruction of the most weakened blocks of the earth's crust, which are accompanied by the formation of sliding boundaries and channels of the statistical functional.
4. As follows from the table, seven out of 15 recorded precursors are located in a relatively narrow interval from 30 to 35 hours before the earthquake, and the same number of precursors are located in a time interval of about 11 hours before this event, which confirms the relationship between the ongoing processes and the reliability of the methodology used.

Thus, we come to the conclusion that the set of the analyzed properties of the statistical functional $L(n)$ can be an indicator of the approaching moment of an earthquake, accompanied by a tsunami. It should be noted that the use of the statistical technique allows not only to fix the set of precursors of the approach of the seismic event, but also to identify time points at which extremely high levels of seismic compression of lithospheric plates in the earthquake preparation zone are achieved with a high probability.

REFERENCES

1. Volvach AE, Kogan LP, Kanonidi KH, Nadezhka LI, Bubukin IT, Shtenberg VB, Gordetsov AS, Krasnikova OV, Kislitsyn DI. Changes in the properties of the statistics of physical and biophysical fields as earthquake precursor. *Communications in Nonlinear Science and Numerical Simulation,* 2022, 108(1):106200-1–106200-18.
2. Volvach AE, Kogan LP, Kanonidi KH, Bubukin IT, Shtenberg VB, Volvach LN, Biazitov DT. Statistical precursors of a strong earthquake on April 6, 2009 on the Apennine Peninsula. *Heliyon*, 2022, 8(8):e10200-1–e10200-22.
3. Kogan LP. Change in statistical functionals of critical frequency prior to strong earthquakes. *Geomagn. Aeron.*, 2015, 55:507-520.
4. Gutenberg B, Richter CF. Frequency of Earthquakes in California. *Bulletin of the Seismological Society of America*, 1944, 34(4):185-188.
5. Gutenberg B and Richter CF. *Seismicity of the Earth and Associated Phenomena*. 2nd ed. Princeton, N.J., Princeton University Press, 1954, 255 p.
6. Amitrano D. Variability in the power-law distributions of rupture events, How and why does b-value change. *Eur. Phys. J.,* 2012, 205:199-215.
7. Popandopoulos GA, Lukk AA. The depth variations in the b-value of frequency-magnitude distribution of the earthquakes in the Garm region of Tajikistan. *Izvestiya. Physics of the Solid Earth*, 2014, 50(2):273-288.

8. Popandopoulos GA. Spatiotemporal variations in Gutenberg–Richter b-value depending on the depth and lateral position in the earth's crust of the Garm region, Tajikistan. *Izvestiya. Physics of the Solid Earth,* 2020, 56(3):337-356.
9. Han Q, Wang L, Xu J, Carpinteri A, Lacidogna G. A robust method to estimate the b-value of the magnitude–frequency distribution of earthquakes. *Chaos, Solitons and Fractals,* 2015, 81(A):103-110.
10. Novopashina AV, Sankov VA. Migracii realizovannoi seismicheskoi energii v razlichnih geodinamicheskih usloviyah. [Migrations of released seismic energy in various geodynamic conditions]. *Geodinamika i Tektonofizika*, 2018, 9(1):139–163 (in Russ.).
11. Gkarlaouni C, Lasocki S, Papadimitriou E, Tsaklidis G. Hurst analysis of seismicity in Corinth rift and Mygdonia graben (Greece). *Chaos, Solitons & Fractals*, 2017, 96(C):30-42.
12. Trofimenko SV, Bykov VG, Merkulova TV. Space-time model for migration of weak earthquakes along the northern bound Seismol. *Journal of Seismology*, 2017, 21:277–286.